THE JOURNAL OF BIOLOGICAL CHEMISTRY VOL. 290, NO. 46, pp. 27959–27971, November 13, 2015

Affinity Purification and Structural Features of the Yeast Vacuolar ATPase V_o Membrane Sector*

Received for publication, April 30, 2015, and in revised form, September 25, 2015 Published, JBC Papers in Press, September 28, 2015, DOI 10.1074/jbc.M115.662494

Sergio Couoh-Cardel, Elena Milgrom, and Stephan Wilkens[1]

From the Department of Biochemistry and Molecular Biology, State University of New York Upstate Medical University, Syracuse, New York 13210

Background: Vacuolar ATPase is regulated by reversible disassembly into V_1-ATPase and the V_o proton channel.
Results: Upon enzyme disassembly, subunit *a* cytoplasmic domain changes conformation to bind subunit *d*.
Conclusion: The conformational change of subunit *a* may play a role in blocking passive proton flow through free V_o.
Significance: The interaction of a_{NT} and *d* in free V_o ensures the efficient reassembly of the holo enzyme.

The membrane sector (V_o) of the proton pumping vacuolar ATPase (V-ATPase, V_1V_o-ATPase) from *Saccharomyces cerevisiae* was purified to homogeneity, and its structure was characterized by EM of single molecules and two-dimensional crystals. Projection images of negatively stained V_o two-dimensional crystals showed a ring-like structure with a large asymmetric mass at the periphery of the ring. A cryo-EM reconstruction of V_o from single-particle images showed subunits a and d in close contact on the cytoplasmic side of the proton channel. A comparison of three-dimensional reconstructions of free V_o and V_o as part of holo V_1V_o revealed that the cytoplasmic N-terminal domain of subunit a (a_{NT}) must undergo a large conformational change upon enzyme disassembly or (re)assembly from V_o, V_1, and subunit C. Isothermal titration calorimetry using recombinant subunit d and a_{NT} revealed that the two proteins bind each other with a K_d of ~5 μM. Treatment of the purified V_o sector with 1-palmitoyl-2-hydroxy-*sn*-glycero-3-[phospho-rac-(1-glycerol)] resulted in selective release of subunit d, allowing purification of a $V_o\Delta d$ complex. Passive proton translocation assays revealed that both V_o and $V_o\Delta d$ are impermeable to protons. We speculate that the structural change in subunit a upon release of V_1 from V_o during reversible enzyme dissociation plays a role in blocking passive proton translocation across free V_o and that the interaction between a_{NT} and d seen in free V_o functions to stabilize the V_o sector for efficient reassembly of V_1V_o.

Vacuolar H^+-ATPases (V-ATPases, V_1V_o-ATPases)[2] are large, multisubunit protein complexes that are found in the endomembrane system of all eukaryotic organisms, where they function to acidify the lumen of intracellular organelles (1–3). In specialized cells of higher eukaryotes, V-ATPases are also found in the plasma membrane, where the enzyme is pumping protons into the extracellular milieu (1, 4). Aberrant V-ATPase function has been shown to be associated with numerous widespread human conditions, including renal tubular acidosis (5), sensorineural deafness (6), osteoporosis (7), diabetes (8), microbial (9) and viral infection (10), infertility (11), and cancer (12). V-ATPase has therefore been deemed a valuable drug target (13–15). However, lack of detailed structural information has limited the application of structure-based drug discovery so far.

V-ATPase can be divided into an ATP-hydrolyzing catalytic headpiece, V_1, and a membrane-embedded proton-translocating sector, V_o. The subunit composition of the enzyme from the model organism *Saccharomyces cerevisiae* is $A_3B_3(C)DE_3FG_3H$ for V_1 (16) and $ac_8c'c''de$ for V_o (17, 18). Crystal structures of the bacterial V_1-ATPase from *Enterococcus hirae* show the three A and B subunits arranged in an alternating fashion around a central cavity within which are located the N- and C-terminal ends of subunit D (19). The proton channel is formed at the interface of the ring of the *c*, *c*′, and *c*″ subunits ("proteolipid" ring) and the C-terminal domain of subunit *a* (a_{CT}) (17, 20). V-ATPase is a member of the family of rotary molecular motor enzymes that, next to V-ATPase, includes F-ATP synthase, found in bacteria, mitochondria, and chloroplasts; archaeal A-ATP synthase; and bacterial A/V-like ATPase (21–23). In eukaryotic V-ATPase, ATP hydrolysis taking place at three catalytic sites located at the interface of the A and B subunits on the membrane extrinsic V_1 is coupled to proton translocation across the V_o via a central rotor formed by the DF heterodimer of the V_1 and the subunit *d*-proteolipid ring subcomplex of the V_o. Three peripheral stalks, formed by subunit EG heterodimers together with the single-copy H and C subunits, form the stator that links the catalytic sector to the membrane-embedded proton channel via a_{NT}, and that functions to withstand the torque generated during rotary catalysis (Fig. 1*A*). However, unlike the related F-, A- and bacterial V-type motors, eukaryotic vacuolar ATPase is regulated by a reversible disassembly and reassembly mechanism employed by the organism to modulate the activity of the complex in

* This work was supported by National Institutes of Health Grant GM058600 (to S. W.). The authors declare that they have no conflicts of interest with the contents of this article.
The 3D cryo-EM reconstruction has been deposited at the EMDB with accession number EMD-2975.
[1] To whom correspondence should be addressed. Tel.: 315-464-8703; Fax: 315-464-8705; E-mail: wilkenss@upstate.edu.
[2] The abbreviations used are: V-ATPase, vacuolar ATPase; DDM, dodecyl maltoside; UnDM, undecyl-β-D-maltoside; LPPG, 1-palmitoyl-2-hydroxy-*sn*-glycero-3-[phospho-rac-(1-glycerol)]; DOPC, 1,2-dioleoyl-*sn*-glycerol-3-phosphocholine; TAP, tandem affinity purification; BME, β-mercaptoethanol; SAXS, small-angle X-ray scattering; MBP, maltose binding protein; ITC, isothermal titration calorimetry; $PI(3,5)P_2$, phosphatidylinositol 3,5-bisphosphate.

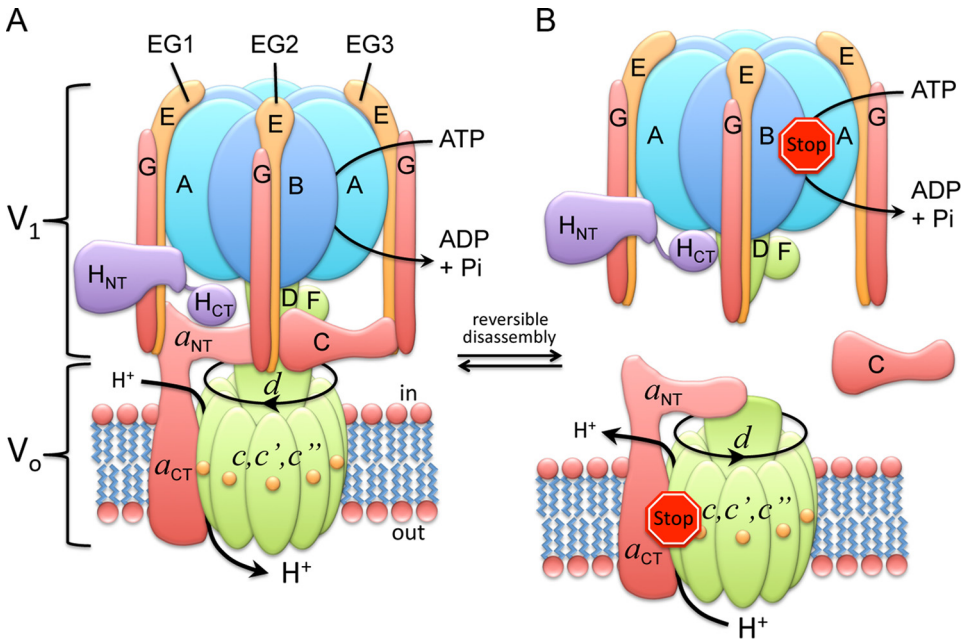

FIGURE 1. **Yeast V-ATPase subunit architecture and regulation by reversible disassembly.** *A*, schematic of yeast V-ATPase subunit architecture. *B*, V-ATPase is regulated by nutrient-dependent reversible disassembly, resulting in V_1 and V_o sectors that have no magnesium ATPase and passive proton translocation activity, respectively. The rotor is shown in *green*, the stator in *red/orange*, the catalytic core in *cyan/blue*, and subunit H in *purple*.

response to, *e.g.*, nutrient availability or developmental state (24, 25). The mechanism of reversible disassembly has been studied extensively in the yeast system, and it is known that V-ATPase dissociation results in a cytoplasmic V_1 and a membrane-bound V_o, with the activity of the two sectors silenced (26, 27) (Fig. 1*B*). In isolated V_1, magnesium ATPase activity is silenced by subunit H, possibly together with inhibitory magnesium ADP (26, 28). The mechanism of blocking passive proton translocation across isolated V_o, however, is less well understood, in part because of a lack of detailed structural information for the eukaryotic V-ATPase membrane sector.

Previously, we obtained three-dimensional reconstructions of free V_o (29) and holo V-ATPase from bovine brain clathrin-coated vesicles (30) and yeast vacuoles (31), and, by fitting available crystal structures into the EM density, we were able to generate a pseudo-atomic model of the enzyme from yeast (31). Recent intermediate-resolution cryo-EM reconstructions of yeast (18, 32) and insect (33) V-ATPase provided additional structural detail and allowed a first view "inside" the membrane sector of the complex.

Here we developed a procedure for purifying the yeast V_o sector amenable for biochemical and biophysical characterization. Electron microscopy of V_o single particles and two-dimensional crystals showed a ring-like structure with additional protein densities at the periphery and cytoplasmic side of the ring. A comparison of the structure of free *versus* holo V-ATPase-bound V_o revealed that enzyme regulation by reversible disassembly involves a large structural rearrangement of a_{NT} from a peripheral position seen in V_1V_o (where a_{NT} interacts with subunit C and the peripheral stator EG2) to a position in free V_o where a_{NT} binds subunit *d*. We speculate that the conformational change in a_{NT} that accompanies V-ATPase dissociation plays a role in activity-silencing in the isolated V_o sector and that the interaction between subunit *d* and a_{NT} seen only in free V_o stabilizes the membrane sector to ensure efficient reassembly of the holo enzyme.

Experimental Procedures

Reagents—Dodecyl maltoside (DDM), undecyl-β-D-maltoside (UnDM), and CHAPS were from Anatrace. 1-palmitoyl-2-hydroxy-*sn*-glycero-3-[phospho-rac-(1-glycerol)] (LPPG), phosphatidylcholine, phosphatidic acid, and 1,2-dioleoyl-*sn*-glycerol-3-phosphocholine (DOPC) were obtained from Avanti. Calmodulin-Sepharose beads were from GE Healthcare or Agilent, and 9-amino-6-chloro-2-methoxyacridine dye was from Invitrogen. The anti-TAP tag polyclonal antibody directed against the amino acid sequence upstream of the tobacco etch virus protease cleavage site was from GenScript. All other reagents were of analytical grade.

Yeast Strains and Growth—Yeast strain YSC1178-7502926 with a TAP tag fused at the C terminus of subunit *a* (a_{TAP}) was from Open Biosystems. To disrupt the subunit B (Vma2p) gene in YSC1178-7502926, a fragment of genomic DNA containing the NAT1 fragment was amplified by PCR from genomic DNA of strain BY4741 vma2Δ::nat1 using oligonucleotides vma2-840 5′-GAATCGGCTAGAGATTACAAC-3′ and vma2-c4 5′-CATGTTCTTCGAGACCGGGTTG G-3′. The resulting 1.2-kb product was used to transform YSC1178-7502926. Transformed colonies were selected on yeast extract (10 g/liter), peptone (20 g/liter), dextrose (20 g/liter) plates supplemented with 100 μg/ml ClonNat (nourseothricin, Werner BioAgents). Colonies were further selected on the basis of their ability to grow on yeast extract, peptone, dextrose buffered to pH 5.0 but not on yeast extract, peptone, dextrose buffered to pH 7.5 + 60 mM $CaCl_2$. Western blot analysis of whole-cell lysates using anti-TAP and anti-subunit B antibodies were performed to confirm the presence and absence of a_{TAP} and subunit B, respectively. The resulting strain was grown in yeast extract,

peptone, dextrose supplemented with 50 mM KH_2PO_4 and 50 mM succinic acid (pH 5). For large-scale biomass production, cells from 8–10 liters of flask culture (A_{600} ~7) were collected by centrifugation, transferred to a 10-liter fermenter, and grown to the second diauxic log phase. Cells were harvested by centrifugation, washed once with distilled water, and stored at −80 °C until use. Final cell weight was 8–10 g/liter of culture.

Isolation of Membranes—All steps were performed at 4 °C unless noted otherwise. Cells were resuspended in lysis buffer (20 mM Tris-HCl, 150 mM NaCl (pH 7.4) (TBS) supplemented with 8% sucrose, 2% sorbitol, and 2% glucose), and an inhibitor mixture was added to a final concentration of 2 μg/ml leupeptin, 2 μg/ml pepstatin A, 0.5 μg/ml chymostatin, and 1 mM PMSF. 1 mM EDTA was added before disrupting cells in a homemade bead beater using 0.5 mm Zirconia beads (BioSpec), keeping the temperature below 14 °C inside the chamber. Cell debris was removed by low-speed centrifugation (1200 × *g*, 10 min), and crude membranes were collected by ultracentrifugation at 130,000 × *g* for 1 h and washed once in lysis buffer. The final membrane pellet was resuspended in the presence of the inhibitor mixture mentioned above. Protein concentration was measured, and membranes were frozen at −80 °C until use.

V_o Purification—Isolated membranes were diluted to a final concentration of 10 mg/ml in lysis buffer, and inhibitor mixture was added. Extraction was carried out by adding DDM from a 20% stock solution in water to a final concentration of 2 mg of detergent/1 mg of protein, followed by gentle stirring for 1 h. Extracted membranes were cleared by ultracentrifugation at 106,000 × *g* for 1 h, and the pellet was discarded. The supernatant was collected carefully, avoiding the upper lipid layer, and $CaCl_2$ was added to a final concentration of 4 mM. The mixture was incubated with 4 ml of Calmodulin beads for 1 h at 4 °C under gentle agitation. The beads were collected in a chromatography column and washed with 20 column volumes of 10 mM Tris-HCl (pH 8), 10 mM β-mercaptoethanol (BME), 2 mM $CaCl_2$, 0.1% DDM, 150 mM NaCl, and 20 column volumes of the same buffer without NaCl. The column was eluted with 10 mM Tris-HCl (pH 8), 10 mM BME, 0.5 mM EGTA, and 0.1% DDM. Fractions were analyzed by 13% SDS-PAGE, and fractions containing V_o were pooled and concentrated in a 100-kDa Vivaspin concentrator (Sartorius Stedim Biotech).

Glycerol Gradient Centrifugation and Removal of Subunit d—1 mg of purified V_o was applied to the top of a discontinuous glycerol gradient (15–35% (v/v), 10 mM Tris-HCl (pH 8), 10 mM BME, 0.5 mM EGTA, and 0.01% phosphatidylcholine:phosphatidic acid (19:1)) and centrifuged at 200,000 × *g* for 16 h at 4 °C. For removal of subunit *d*, 0.05% LPPG was included in the gradient. Otherwise, 0.5% CHAPS was used. Fractions were collected from the bottom and analyzed by SDS-PAGE.

Reconstitution in Liposomes—200 μg of V_o (in CHAPS) or subunit *d*-depleted V_o ($V_o\Delta d$) (in LPPG) was mixed with 15 mg of phosphatidylcholine:phosphatidic acid (19:1 v/v) and adjusted with CHAPS to 6%. In some experiments, 9% ergosterol was included in the reconstitution mix. Samples were applied to a Sephadex G50 column (50 cm × 1.6 cm) and eluted with high-potassium buffer (20 mM HEPES (pH 7), 2 mM BME, 0.2 mM EGTA, 10% glycerol, 100 mM K_2SO_4, and 0.5 mg/ml fatty acid-free BSA) at a flow rate of 0.5 ml/min. The eluate was collected in 1-ml fractions, and turbid fractions were analyzed by 13% SDS-PAGE and silver staining.

Passive Proton Translocation Assay—Proton translocation assays were performed as described by Qi and Forgac (34). Briefly, assays were conducted in a 3-ml cuvette. 30 μl of each fraction was preincubated in high-sodium buffer (20 mM HEPES (pH 7), 2 mM BME, 0.2 mM EGTA, 10% glycerol, 150 mM NaCl, and 0.5 mg/ml fatty acid-free BSA) for 5 min at 30 °C in the presence of 2 μM 9-amino-6-chloro-2-methoxyacridine. After 300-s incubation, the process was started by addition of 1 μM valinomycin, followed by 1 μM carbonyl cyanide *p*-trifluoromethoxyphenylhydrazone. Different fractions were probed after 1, 4, and 10 days. Six independent preparations of V_o and V_o-*d* were analyzed.

Flotation Assays—To verify lipid vesicle reconstitution of V_o and V_o-*d*, fractions from the G50 column (fraction 29 for V_o and fraction 28 for V_o-*d*) were adjusted with sucrose to 53% and placed in the bottom of an 11-ml tube. A sucrose step gradient (40, 20, and 0% (w/v) in 20 mM HEPES (pH 7), 2 mM BME, 0.2 mM EGTA, 10% glycerol, and 150 mM NaCl) was layered on top of the V_o sample and centrifuged at 200,000 × *g* for 16 h at 4 °C. Fractions were collected from the top of the tube and analyzed by 13% SDS-PAGE and silver staining.

Mass Spectrometry of V_o Subunits—The V_o sector was precipitated with 1% trichloroacetic acid, and the centrifuged pellet was washed with water. The pellet was extracted with a 1:1 mixture of water and trifluoroethanol, and the soluble fraction was analyzed by electrospray ionization mass spectrometry using a Q-TOF Micro mass spectrometer (Waters, Inc.) in positive ion mode. Charge envelopes between 800–2500 *m*/*z* were deconvoluted using MaxEnt2 as implemented in MassLynx4.1. Calibration of the instrument was carried out with phosphoric acid and sodium/cesium iodide. Analysis of gel bands by peptide sequencing was done at the Upstate Medical University mass spectrometry core facility using a Thermo LTQ Orbitrap mass spectrometer.

Small-angle X-ray Scattering Analysis—Small-angle x-ray scattering (SAXS) data were collected at the Cornell High-energy Synchrotron Source (MacCHESS) F2 beam line operating at a wavelength of 1.2524 Å at 4 °C. For SAXS data collection, V_o was purified using UnDM instead of DDM. V_o was diluted into 10 mM Tris-HCl (pH 8), 10 mM BME, 0.5 mM EGTA, and 0.05% UnDM to 1, 2, 4, 6, 8, and 10 mg/ml. 30-μl samples were exposed twice for 180 s without an obvious decay in signal. Signal averaging, buffer subtraction and Guinier analysis were done in Bioxtas RAW (35). Molecular weight was estimated using lysozyme as the standard. Thirty data points were used for Guinier analysis for each tested concentration (*qRg* was ~1.1 in all cases).

Two-dimensional Crystallization and EM Analysis—Purified V_o was diluted to 3 mg/ml in 10 mM Tris-HCl (pH 6.5), 10 mM BME, 0.5 mM EGTA, 10% glycerol, and 1 mM DTT, and sonicated DOPC was added to reach a lipid-to-protein ratio of 0.3 (w/w). After 24 h, the detergent was removed by stepwise addition (every 3 days) of equal amounts of polystyrene beads (Bio Beads SM2, Bio-Rad) for a total of 10 days so that the final ratio of beads to liquid was ~1:1. Samples were kept at 4 °C, and 1 mM sodium azide was added to inhibit bacterial growth. V_o

two-dimensional crystals were spotted on glow discharge-treated, carbon-coated copper grids and stained with 1% uranyl acetate. Micrographs were recorded on a 4096 × 4096 charge-coupled device (TVIPS F415MP) at ×20,000–40,000 electron optical magnification and an underfocus of 1.5 μm. The quality of the crystalline areas was assessed from calculated power spectra, and areas showing isotropic reflections to ~20-Å resolution were excised and analyzed with the 2dx package of programs (36) and/or by correlation averaging as implemented in IMAGIC 5 (37, 38).

Cryo EM and Single-particle Image Analysis—The solubilized V_o sector was vitrified at 1–2 mg/ml on glow-discharged, holey, carbon-coated copper grids (C-flat, 2/2 μm). Grids were mounted in a Gatan 626 cryoholder and imaged in a JEOL JEM-2100 transmission electron microscope operating at 120 kV. Micrographs were recorded on a 4096 × 4096 charge-coupled device (TVIPS F415MP) at an electron optical magnification of ×40,000 and an underfocus of between 1.5–2.5 μm. The calibrated pixel size on the specimen level was 2.62 Å. A total of 12,035 particles was extracted as 144 × 144 pixel images using the "boxer" program of the EMAN1.9 software package (39). The dataset was contrast transfer function-corrected using "ctfit" as implemented in EMAN1.9. All subsequent image analysis was done with the IMAGIC 5 package of programs (37). Images were bandpass-filtered to remove low ($<6.4 \times 10^{-3}$ $Å^{-1}$) and high (>0.15 $Å^{-1}$) spatial frequencies, and a soft-edge circular mask was applied before subjecting the images to reference-free alignment (40). Averages from the reference-free alignment were then used in subsequent multireference alignment, and the multireference alignment was iterated to obtain averages of the most abundant projections. Three-dimensional reconstruction was initiated by one round of projection-matching using the low pass-filtered three-dimensional reconstruction of the bovine V-ATPase membrane sector (29) as a reference model. Because the bovine V_o sector subunit Ac45 is not found in yeast V_o, the density corresponding to Ac45 was removed with the volume eraser tool as implemented in the visualization software Chimera (41). Cycles of projection-matching alignment and three-dimensional reconstruction were iterated with increasing numbers of references until no further improvement was observed. The resolution of the final model was estimated using the 0.5 Fourier shell correlation criterion (42). The final EM density was fitted manually with crystal structures of bacterial homologs for the yeast V_o subunits, including the a_{NT} homolog from *Meiothermus ruber* (I_{NT}, PDB code 3RRK), the subunit *d* homolog from *Thermus thermophilus* (subunit C, PDB code 1R5Z), and the *c* subunit ring homolog from *E. hirae* (K_{10}, PDB code 2BL2). Although the primary sequence conservation between the yeast and bacterial subunits is limited (11%, 16%, and 26% for a_{NT} and I_{NT}, *d* and C, and *c* and K, respectively), their secondary and tertiary structure is highly conserved, as evidenced by the fact that the yeast subunit structures can be modeled on the basis of the bacterial A/V-ATPase subunit crystal structures using the Phyre2 server (43) with 100% confidence.

Expression and Purification of $a_{NT(1–372)}$ and Subunit d—Plasmid pRS316 containing the open reading frame for subunit *d* (Vma6p) was as a gift from the laboratory of Dr. Karlett Parra (University of New Mexico). The coding sequence for subunit *d* was PCR-amplified using primers GCTCAGGT ACCGATGG-AAGGCGTGTATTTCAATATT (forward) and CGAGTCC-TGCAGTCAATCAATAAACG GAAATATAATT (reverse), and the resulting PCR product was ligated into pGEM T-easy. Subsequent cloning of the subunit *d* coding sequence into a modified plasmid pMAL-c2e (New England Biolabs, enterokinase cleavage site replaced by the human rhinovirus 3C site) for bacterial protein expression was done by BioBasic, Inc. (Markham, Ontario). The resulting construct consisted of subunit *d* with an N-terminal fusion of maltose binding protein (MBP) separated by a protease cleavage site (human rhinovirus 3C protease) for removal of MBP. pMAL-c2E harboring MBP subunit *d* was expressed in *Escherichia coli* strain Rosetta2. Cells were grown in rich broth (Lennox broth plus 0.2% glucose) to an A_{600} of 0.6 and induced with 500 μM isopropyl 1-thio-β-D-galactopyranoside for 4 h at 37 °C. Purification was done following the recommended protocol for MBP-tagged proteins (New England Biolabs). The PreScission Protease-cleaved (GE Healthcare) fusion was dialyzed against 25 mM Tris-HCl, 1 mM EDTA, 1 mM tris(2-carboxyethyl)phosphine (pH 7), followed by anion exchange chromatography on a 1-ml mono Q-Sepharose column attached to an AKTA FPLC (GE Life Sciences). Under these buffer conditions, subunit *d* bound to the column and was eluted using a 0–500 mM sodium chloride gradient in the same buffer. Protein-containing fractions were pooled, concentrated to 1–2 ml, and subjected to size-exclusion chromatography over Superdex S75 (16 × 500 mm). An expression construct for the N-terminal domain of subunit *a* (Vph1p) consisting of residues 1–372 ($a_{NT(1–372)}$) was generated as described previously (44). The cleavable MBP tag resulted in an N-terminal extension for both subunit *d* and $a_{NT(1–372)}$ constructs with the amino acid sequence GPKVP. Constructs were confirmed by DNA sequencing. A detailed biochemical and biophysical characterization of recombinant subunit *d* and $a_{1–372}$ will be presented elsewhere.

Isothermal Titration Calorimetry (ITC)—ITC measurements of the interaction of $a_{NT(1–372)}$ with subunit *d* using a Microcal VP-ITC isothermal titration calorimeter were done as described previously (44, 45), with the following modifications. Prior to the titration, both proteins were dialyzed (in the same container) against 2 liters of 25 mM Tris-HCl (pH 7), 0.5 mM EDTA, and 1 mM tris(2-carboxyethyl)phosphine. $a_{NT(1–372)}$ was concentrated to 375 μM and titrated into 25 μM subunit *d* at 10 °C using a total of 30 injections with 10.7% saturation/injection. A heat of dilution titration of 375 μM $a_{NT(1–372)}$ into dialysis buffer was subtracted from the $a_{NT(1–372)}$ into subunit *d* titration. A second titration was carried out with 320 μM $a_{NT(1–372)}$ in the syringe using, again, 25 μM subunit *d* in the ITC cell. Both titrations produced very similar results. Protein concentrations were determined from A_{280} using calculated extinction coefficients. ITC data were fitted to a one-site model using the VP-ITC programs in Originlab.

Other Methods—Membrane protein concentrations were measured by BCA method (Thermo Scientific) and improved by TCA precipitation as in Lowry-TCA (46) using fatty acid-free BSA as the standard.

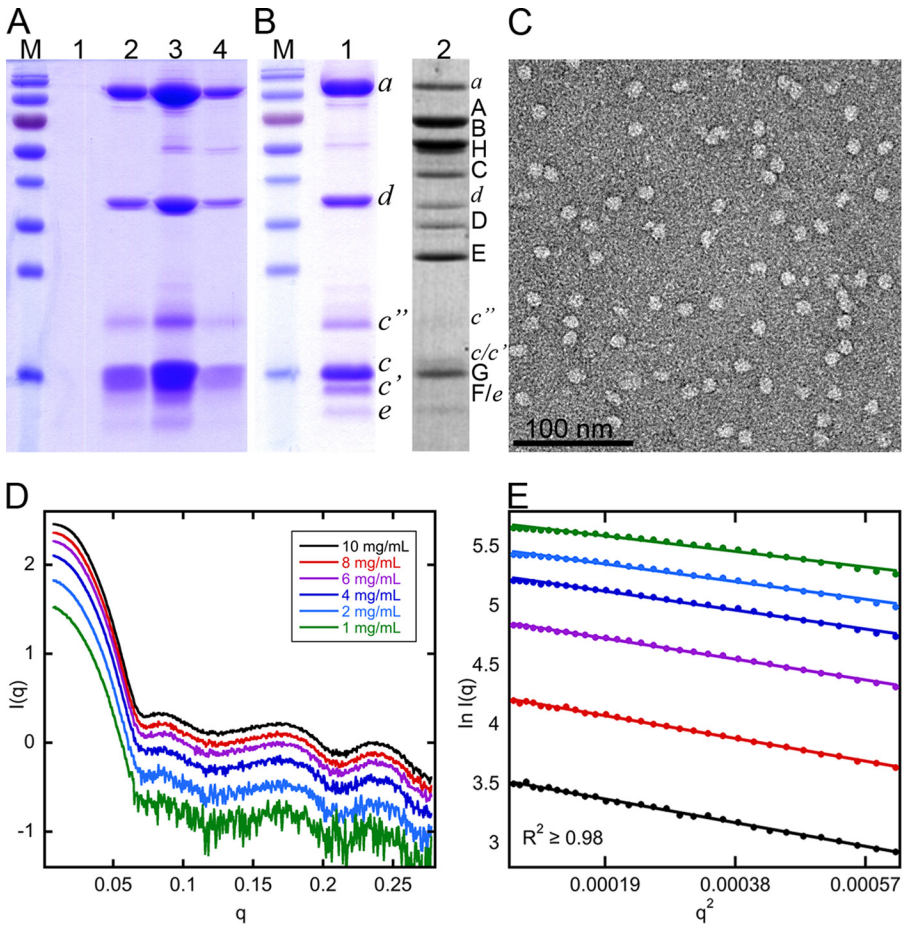

FIGURE 2. **Purification of the yeast V-ATPase V_o domain.** Yeast V_o is purified by way of a calmodulin binding peptide tag fused to the C terminus of subunit *a* (Vph1p) using a yeast strain deleted for subunit B (vma2Δ). The yield of the V_o sector is ~2–3 mg/150 g of cells. *A*, SDS-PAGE of fractions 1–4 eluted from the calmodulin affinity column (10 μg loaded). *M*, molecular mass marker from top to bottom, 170, 130, 100, 70, 55, 40, 35, 25, 15 kDa. *B*, V_o-containing fractions were pooled and concentrated, and 10 μg was resolved on SDS-PAGE and stained with Coomassie Blue (*lane 1*). For comparison, *lane 2* shows SDS-PAGE of the V_1V_o holo enzyme (modified from Ref. 47). *C*, transmission electron microscopy of V_o spotted onto glow-discharged, carbon-coated copper grids at 20 μg/ml and stained with 1% uranyl acetate. *D*, SAXS analysis of the V_o sector at concentrations between 1–10 mg/ml in UnDM-containing buffer. *E*, Guinier analysis of the scattering profiles shown in *D*. The calculated radius of gyration is 51 ± 3.5 Å. The transmission electron microscopy image and SAXS data show that the preparation is homogenous and monodisperse at a concentration of up to 10 mg/ml.

Results

Purification of the V_o Proton Channel Sector—To isolate the yeast V_o sector for structural and functional studies, we attempted several strategies, including C- and N-terminal histidine tags fused to subunits *d* and *c*″ as well as a TAP tag fused to the C terminus of subunit *a* or *c*. In the end, the best results were obtained using only the second affinity step of the TAP procedure, where V_o (containing TAP-tagged subunit *a*) is detergent-solubilized from vacuolar membranes and captured by a calmodulin column by way of the calmodulin binding peptide in the tag. To eliminate possible co-purification of (partially) assembled V-ATPase, the gene for V_1-ATPase subunit B (VMA2) was disrupted. For large-scale purification of the vacuolar ATPase membrane sector, yeast was grown in a 10-liter fermenter. The yield of V_o sector purified as described under "Experimental Procedures" was ~2–3 mg/150 g of cells. Fig. 2 summarizes the purification of the yeast V-ATPase V_o sector and characterization of the protein by negative-stain transmission electron microscopy and SAXS. Fig. 2*A* shows SDS-PAGE of fractions 1–4 eluted from the calmodulin column. The Coomassie-stained gel shows bands for subunits *a*, *d*, *c*″, *c*, *c*′, and *e*. Fig. 2*B* shows SDS-PAGE of the final preparation obtained after concentrating fractions 2–4 of the calmodulin column (*lane 1*, 10 μg of protein loaded), and *lane 2* shows SDS-PAGE of holo V-ATPase (47) for comparison. Mass spectrometry analysis of the subunit *a* band from SDS-PAGE gels such as shown in Fig. 2, *A* and *B*, only produced subunit *a*-derived peptides, with no peptides from protein A being detected, indicating that the protein A moiety of the TAP tag was lost because of proteolytic degradation following cell lysis and detergent extraction of membranes. Loss of protein A was confirmed by immunoblot analysis (using an antibody directed against the C-terminal end of the calmodulin binding peptide) that showed that the apparent molecular mass of the subunit *a* band decreased in size from an initial ~130 kDa at the washed membrane stage to the final ~116 kDa after the elution from the calmodulin affinity column (data not shown). Electrospray ionization/TOF mass spectrometry analysis of denatured V_o revealed the presence of proteins with masses of 39,903 Da (subunit *d*, expected 39,791 Da), 16,255 Da (subunit *c*, expected 16,219 Da), and 8,250 Da (subunit *e*, expected 8,249 Da). The mass differences suggest N-terminal acetylation for subunit *c* and an ~100-Da modification

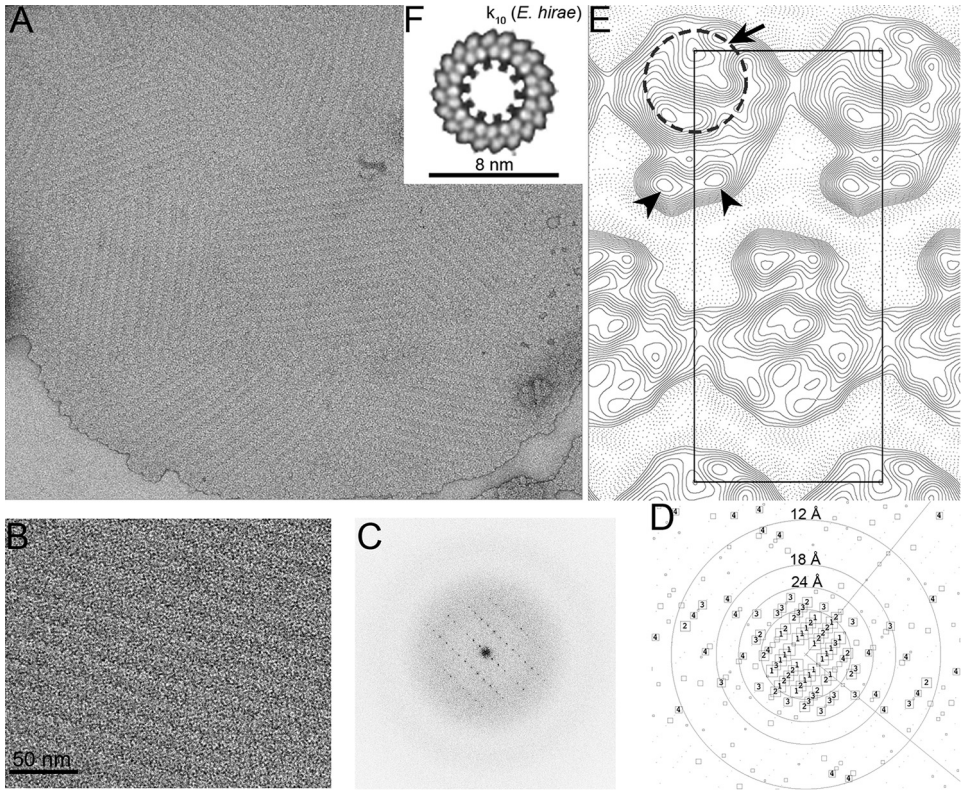

FIGURE 3. **Electron crystallography of yeast V_o sector two-dimensional crystals.** The two-dimensional crystals were obtained by mixing purified V_o at 3 mg/ml with 1 mg/ml DOPC with subsequent removal of detergent (DDM) with polystyrene beads. *A*, overview of a large, single-layer sheet of reconstituted V_o containing several crystalline domains (negatively stained with 1% uranyl acetate). *B*, larger view of a crystalline area, with the power spectrum shown in *C*. *D*, IQ plot after unbending using the 2dx package of programs (36). *E*, projection map with unit cell outlined by the *rectangle*. The cell dimensions are 101 × 236 Å with 2 molecules/cell. The crystals belong to plane group P1 with alternating up and down orientation of the molecules. At the current resolution of ~24 Å, the projections obtained in negative stain show a ring-like structure (*arrow*) with a two-domain asymmetric mass at the periphery (*arrowheads*). We interpret the ring to represent the proteolipid ring and the asymmetric mass a_{CT}. *F*, cross-section of the *E. hirae* K_{10} ring as seen perpendicular to the plane of the membrane, filtered to a resolution of 16 Å.

for subunit *d*. Possibly because of their large size or lower abundance, no peaks for subunits *a* (100,143 Da without protein A), *c*′ (16,902 Da), and *c*″ (22,464 Da) were observed in the deconvoluted charge series (data not shown).

Fig. 2*C* shows negative-stain transmission electron microscopy analysis of detergent-solubilized V_o. The image shows homogeneously sized particles with a diameter of ~10–15 nm, indicating that the preparation contains intact V_o sectors that are stable in the detergent used for purification (DDM). Furthermore, Guinier plots of small angle x-ray scattering profiles obtained from solutions of V_o sector purified in UnDM (chosen here for its smaller micelle size) showed that the preparation is monodisperse at concentrations of up to 10 mg/ml. The molecular mass of V_o as estimated by SAXS was 544 ± 33 kDa, with a calculated radius of gyration of ~51 ± 3.5 Å. The expected mass of V_o (assuming a subunit ratio of $ac_8c'c''de$, see next paragraph and "Discussion") is ~320 kDa, resulting in a difference between the measured and expected mass of ~244 kDa. Considering the average size of UnDM micelles of 35 kDa (micelle size reported by Anatrace) suggests that each V_o sector binds six to seven detergent micelles. Taken together, the data show that highly purified, stable, and monodispersed yeast V_o sector can be obtained via affinity chromatography using a calmodulin peptide fused to the C terminus of subunit *a*.

Two-dimensional Crystallization of the Yeast V_o Sector—Fig. 3 summarizes the transmission electron microscopy analysis of yeast V_o domain two-dimensional crystals. The two-dimensional crystals were obtained by mixing the purified V_o domain at 3 mg/ml with 1 mg/ml DOPC, followed by removal of detergent (DDM) using polystyrene beads over a period of 7–10 days. V_o two-dimensional crystals were visualized by negative-stain transmission electron microscopy, and images showing crystalline areas (Fig. 3, *A* and *B*) with reflections in calculated power spectra extending to the first zero of the contrast transfer function (~24 Å; Fig. 3, *C* and *D*) were processed as described under "Experimental Procedures." The crystals belong to plane group P1 with an alternating up and down orientation of the molecules, as evident from the final projection map shown in Fig. 3*E*. At the current resolution of ~24 Å, the projections obtained in negative stain show a ring-like structure with a diameter of 8.5 nm and an asymmetric mass at its periphery (*arrow* and *arrowheads*, respectively, Fig. 3*E*). We interpret the ring to represent the proteolipid ring (for comparison, see the low pass-filtered projection of the *E. hirae* K_{10} ring (PDB code 2BL2 (48), shown in Fig. 3*F*) and the asymmetric mass a_{CT}. As can be seen in Fig. 3, *E* and *F*, both rings are of equal size, consistent with the now established number of 10 proteolipids in the yeast enzyme (18). Taken together, the data show that the detergent-solubilized yeast V-ATPase V_o sector can be lipid-reconstituted and crystallized in two dimensions, opening a path for high-resolution structure determination of the V-ATPase membrane sector in its native environment.

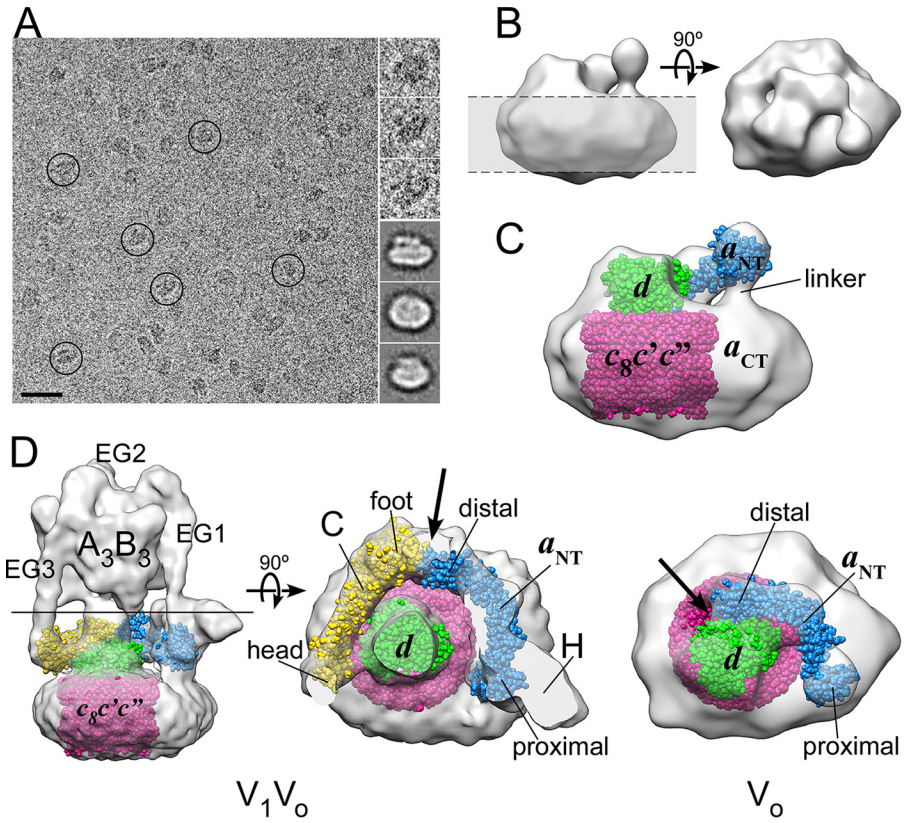

FIGURE 4. **Three-dimensional reconstruction of the yeast V_o sector from cryo-EM.** *A*, the purified yeast V_o domain was vitrified at a concentration of 2 mg/ml and visualized at −170 °C. Individual side view projections are shown at the *top right*, and averages obtained by reference-free alignment of characteristic side and top views are shown at the *bottom right*. *Bar* = 20 nm. *B*, side view (*left*) and top view (*right*) of the three-dimensional reconstruction of yeast V_o calculated from a dataset of ~12,000 single molecules at a resolution of ~18 Å. The *gray rectangle* in the side view indicates the position of the lipid bilayer. *C*, fitting of crystal structures into the EM reconstruction. The structural models used were the a_{NT} homolog from *M. ruber* (PDB code 3RRK, *blue*), the subunit *d* homolog from *T. thermophilus* (PDB code 1R5Z, *green*), and the K_{10} proteolipid ring from *E. hirae* (PDB code 2BL2, *magenta*). *D*, side view (*left panel*) and cross-section (*center panel*) of holo yeast V-ATPase cryo-EM reconstruction (emd-5476 (32)) for comparison. In free V_o (*right panel*, *arrow*), the "distal" end of a_{NT} is in contact with subunit *d*, whereas, in holo V_1V_o, the distal domain of a_{NT} is in a more peripheral position in contact with C_{foot} and EG2 (*center panel*, *arrow*). For details, see text.

Cryo-electron Microscopy and Three-dimensional Reconstruction—Fig. 4 summarizes single-molecule cryo-transmission electron microscopy analysis of the detergent-solubilized V_o sector. V_o was vitrified at a concentration of 2 mg/ml, and charge-coupled device (CCD) images were recorded at a magnification of ×40,000 (Fig. 4*A*). Three enlarged raw images of particles and three averages of aligned projections in the typical "side" and "top" view orientations are shown next to the micrograph. A dataset of 12,035 single-particle images was used to generate a three-dimensional model, starting with projections of the low pass-filtered three-dimensional reconstruction of the bovine V_o sector (29) as initial references, followed by multiple rounds of projection-matching refinement. The resolution of the final model (Fig. 4*B*) was estimated to be ~18 Å on the basis of the 0.5 Fourier shell correlation criterion using models calculated from half-data sets (data not shown). The yeast V_o sector is composed of a ring of 10 proteolipids (likely $c_8c'c''$, see "Discussion"), the 100-kDa *a* subunit that is equally divided into a cytoplasmic a_{NT} and a membrane integral a_{CT} that is bound at the periphery of the proteolipid ring, the ~40 kDa *d* subunit that is bound at the cytoplasmic rim of the proteolipid ring (Fig. 4*C*), and subunit *e*, which is likely bound to a_{CT} (49). Because there are no x-ray crystal structures available for any of the yeast polypeptides, the EM model was fitted with crystal structures of the homologous subunits of related bacterial rotary ATPases: the K_{10} ring from *E. hirae* (PDB code 2BL2 (48)), I_{NT} from *M. ruber* (PDB code 3RRK (50)), and the subunit *d* homolog from *T. thermophilus* (PDB code 1R5Z (51)). A comparison with the negative-stain three-dimensional model of the bovine V_o (29) revealed an overall similar architecture except for the presence of density for Ac45 on the luminal side of the bovine model (a homolog for Ac45 is not present in yeast) and the presence of density for the linker (or tether) connecting a_{NT} and a_{CT} in the yeast cryo-EM model (Fig. 4*C*). At the current resolution of ~18 Å, the proteolipid ring within the membrane domain is not clearly resolved, likely because of the small size of the relatively featureless complex and the lack of internal symmetry. Well resolved, however, are a_{NT} and subunit *d*, which are situated on the cytoplasmic side of the membrane.

Comparison of EM Reconstructions of the Isolated V_o and V_o Sector as Part of Holo V-ATPase—As can be seen in Fig. 4*C*, fitting the crystal structures of the bacterial homologs of yeast a_{NT} (PDB code 3RRK (50)) and subunit *d* (PDB code 1R5Z (51)) into the yeast V_o EM density shows an interaction of the distal lobe of a_{NT} with the *d* subunit (Fig. 4*D*, *right panel*, *arrow*), with subunit *d* binding slightly off-center at the edge of the proteolipid ring. Interestingly, a comparison with the three-dimensional reconstruction of holo yeast V-ATPase (18, 31, 32) (Fig.

4*D*, *left* and *center panels*) reveals that a_{NT} in the holo enzyme adopts a different conformation where the distal domain of a_{NT} is bound to C_{foot} (subunit domain nomenclature as in Refs. 50 and 52, respectively) and the N termini of one of the three EG heterodimer peripheral stalks (EG2; Fig. 4*D*, *center panel*, *arrow*). In line with this observation, we have previously characterized the binding interactions between a_{NT}, C_{foot}, and the EG heterodimer and we found that these interactions are of moderate affinity (44). Taken together, the comparison of V_o and holo V_1V_o suggests that a_{NT} undergoes a large conformational rearrangement upon enzyme disassembly, going from a conformation in free V_o that binds the *d* subunit to a more peripheral conformation that binds C_{foot} and EG2 in holo V_1V_o.

In Vitro Interaction of Recombinant Subunit d and $a_{NT(1–372)}$—To test whether the interaction between a_{NT} and subunit *d* as seen in the EM reconstruction is specific and can be quantified *in vitro*, we performed ITC experiments with recombinant subunits. For these experiments, subunit *d* and $a_{NT(1–372)}$ were expressed in *E. coli* as N-terminal fusions with MBP and affinity-purified on amylose resin. MBP was cleaved, and the resulting subunits were further purified using ion exchange and size-exclusion chromatography. Fig. 5*A* shows SDS-PAGE of $a_{NT(1–372)}$ (*lane 1*) and subunit *d* (*lane 2*). Both proteins are stable and highly soluble at pH 7, and, although recombinant subunit *d* elutes with an apparent molecular mass of ~42 kDa from a S200 gel filtration column (expected, 40,267 Da), suggesting a globular monomeric protein, $a_{NT(1–372)}$ exists in a concentration-dependent monomer-dimer equilibrium, as already described for the shorter $a_{NT(104–372)}$ construct (Ref. 44) and data not shown). Fig. 5*B* shows a representative ITC experiment in which 375 μM $a_{NT(1–372)}$ was titrated into 25 μM subunit *d*. As can be seen from the titration, complex formation between $a_{NT(1–372)}$ and subunit *d* was exergonic, and fitting the data to a one-site model revealed an N value of 0.98 (consistent with a 1:1 stoichiometry of complex formation), a K_a of $2.1 \times 10^5 \pm 3.5 \times 10^4$ M^{-1} (K_d, ~4.8 μM), a ΔH of -4.2 ± 0.22 kcal/mol, a ΔS of 9.7 cal/(K·mol), and a ΔG of -6.9 kcal/mol. After the titration, the ITC cell content was resolved by gel filtration (S200, 16 × 500 mm), and fractions were analyzed by SDS-PAGE (Fig. 5*C*). As can be seen from the gel, $a_{NT(1–372)}$ and subunit *d* co-elute around fraction 31 (62 ml), corresponding to an apparent molecular mass of ~72 kDa (84 kDa expected for the $a_{NT(1–372)}$-*d* complex; subunit *d* alone elutes at an apparent molecular mass of ~42 kDa, see above). Together, the ITC and gel filtration data suggest that subunit *d* and $a_{NT(1–372)}$ bind each other in a specific manner, albeit with moderate affinity.

Preparation and Functional Analysis of the $ac_8c'c''e$ *Subcomplex* ($V_o\Delta d$)—In living cells, V-ATPase activity is regulated by reversible dissociation into V_1-ATPase and membrane integral V_o sectors (Fig. 1*B*). Upon enzyme dissociation, the activity of both V_1 and V_o is silenced so that V_1 loses the ability to hydrolyze magnesium ATP and V_o becomes impermeable to protons. Considering the interaction described above between a_{NT} and subunit *d* seen in free V_o but not V_1V_o, we speculated that this interaction may contribute to the inhibition of passive proton translocation through isolated V_o by blocking rotation of the *c*-ring past a_{CT}. To assess the role subunit *d* might be playing in blocking proton translocation through isolated V_o, we developed a procedure to selectively remove subunit *d* from V_o to generate the $ac_8c'c''e$ subcomplex ($V_o\Delta d$). Fig. 6, *A* and *B*, shows SDS-PAGE of glycerol density centrifugation of V_o sector in presence of the ionic detergent LPPG and CHAPS, respectively. As can be seen from Fig. 6*A*, in the presence of LPPG, subunit *d* remains at the top of the gradient separated from $ac_8c'c''e$, whereas, in CHAPS, subunit *d* migrates as part of intact V_o. To determine whether removal of subunit *d* allows passive proton

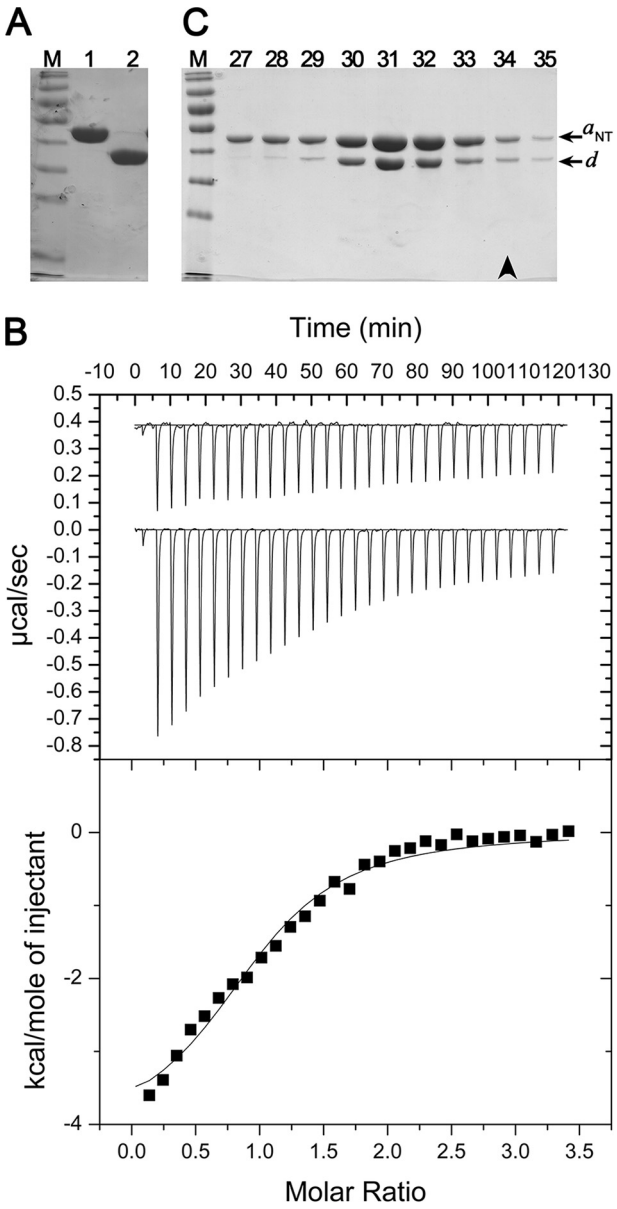

FIGURE 5. **Isothermal titration calorimetry of the a_{NT}-subunit *d* interaction.** *A*, SDS-PAGE of bacterially expressed a_{NT} (residues 1–372, *lane 1*, 5 μg) and subunit *d* (*lane 2*, 5 μg). *M*, molecular mass marker from top to bottom, 170, 130, 100, 70, 55, 40, 35, 25, 15 kDa. *B*, subunit *d* at a concentration of 25 μM in 25 mM Tris/HCl (pH 7), 0.5 mM EDTA, and 1 mM tris(2-carboxyethyl)phosphine was titrated with 375 μM $a_{NT(1–372)}$ in the same buffer. Fitting the ΔH data to a one-site binding model revealed a close to 1:1 binding stoichiometry ($n = 0.98$), a K_a of $2.1 \times 10^5 \pm 3.5 \times 10^4$ M^{-1} (K_d, ~4.8 μM), a ΔH of -4.2 ± 0.22 kcal/mol, a ΔS of 9.7 cal/(K·mol), and a ΔG of -6.9 kcal/mol. *C*, the ITC cell content was resolved by gel filtration over Superdex S200 (16 × 500 mm), and fractions were analyzed by SDS-PAGE. The *arrowhead* (fraction 34) indicates where subunit *d* alone elutes from the column.

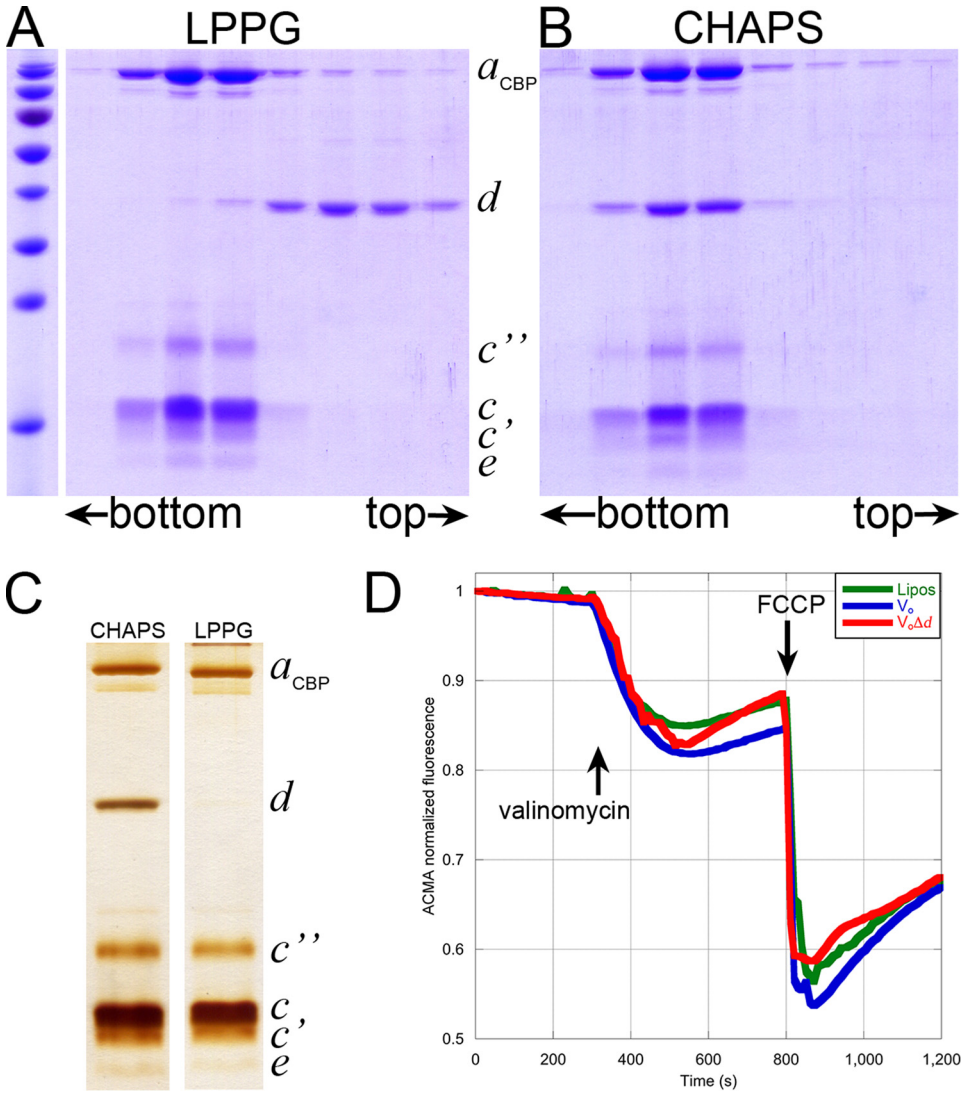

FIGURE 6. **Preparation and functional characterization of $V_o\Delta d$.** *A* and *B*, Coomassie-stained SDS-PAGE of glycerol density gradient centrifugation fractions of V_o in the presence of LPPG (*A*) and CHAPS (*B*). Gradient centrifugation in the presence of LPPG resulted in selective release of subunit *d*, whereas, in the presence of CHAPS, V_o migrates as a homogeneous complex. *C*, V_o and $V_o\Delta d$ in CHAPS were reconstituted at a high lipid:protein ratio using gel filtration (Sephadex G50) in the presence of potassium chloride-containing buffer. Liposomes were collected by centrifugation and subjected to SDS-PAGE and silver staining. *D*, fluorescence-based assay for passive proton translocation. V_o, $V_o\Delta d$, and control liposomes prepared in high-potassium buffer were diluted into sodium-containing buffer in the presence of 9-amino-6-chloro-2-methoxyacridine (*ACMA*), and, after 5 min, a proton gradient was generated by the addition of the potassium ionophore valinomycin. The presence of a proton gradient was subsequently confirmed by addition of the protonophore carbonyl cyanide *p*-trifluoromethoxyphenylhydrazone. Both V_o and $V_o\Delta d$ showed essentially the same behavior as control liposomes, indicating that removal of subunit *d* did not result in passive proton translocation activity.

translocation through the resulting $V_o\Delta d$, V_o and $V_o\Delta d$ were reconstituted into liposomes in the presence of potassium chloride-containing buffer. Liposomes were collected by centrifugation and subjected to SDS-PAGE and silver staining (Fig. 6*C*). V_o- and $V_o\Delta d$-containing liposomes were subjected to a fluorescence-based assay to test for passive proton conductance. Fig. 6*D* shows a representative assay for passive proton conductance. As can be seen from the Fig. 6*D*, both V_o- and $V_o\Delta d$-containing liposomes as well as control liposomes showed the same slow quenching upon addition of the potassium ionophore valinomycin and a sharp drop in the fluorescence signal following addition of the protonophore carbonyl cyanide *p*-trifluoromethoxyphenylhydrazone, which verified the presence of a proton gradient. This result indicates that removal of subunit *d* does not alleviate the inhibition of proton translocation across the V_o, suggesting that the interaction of a_{NT} and subunit *d* in free V_o is not (solely) responsible for activity silencing in the isolated V-ATPase membrane sector.

Discussion

Transmembrane proton transport across the vacuolar ATPase V_o sector involves rotation of the proteolipid ring past a_{CT}. A major difference between eukaryotic vacuolar ATPase and the related F- and A-type motors is the mode of regulation of V-ATPase, which involves dissociation into free ATPase and proton channel sectors triggered by nutrient availability or developmental cues (Fig. 1). However, unlike F- and bacterial A/V-like ATPase ion channels, which, when detached from the ATPase, catalyze passive transmembrane proton transport (53, 54), the eukaryotic V_o sector becomes impermeable to protons

upon dissociation of the V_1, preserving any existing proton gradient across the organellar membrane (55). In case of the F-ATPase ion channel, F_o, it has been shown that rotation of the proteolipid ring relative to the *a* subunit is essential for passive proton conductance (56), and, because the mechanism of ion transport is highly conserved between F- and V-type motors, that means that rotation of the proteolipid ring in free V_o appears to be blocked by an unknown mechanism. Previously, we generated an EM reconstruction of free V_o sector from bovine brain V-ATPase that suggested an interaction between a_{NT} and subunit *d*, although the linker connecting a_{NT} and a_{CT} was not resolved in the negative stain model (29). Later, we (57) and others (34) speculated that the interaction between a_{NT} and *d* may serve to silence passive proton transport by linking the rotor and stator of the motor. To address the mechanism of activity silencing as well as other aspects of V_o structure and function, we developed a protocol to isolate milligram amounts of yeast V_o proton channel sector using affinity chromatography. Biochemical experiments show that the complex is stable in low and intermediate critical micelle concentration (cmc) detergents such as UnDM, DDM, and CHAPS, respectively, as evident from glycerol gradient centrifugation. Negative-stain and cryo-electron microscopy as well as small-angle x-ray scattering experiments show that detergent-solubilized yeast V_o is monodisperse at concentrations up to several milligrams per milliliter, a prerequisite for structural studies.

We next used transmission electron microscopy of two-dimensional crystals and single V_o molecules to obtain structural information that may provide clues regarding the mechanism of activity silencing. Upon reconstitution into DOPC lipid bilayers, we were able to generate two-dimensional crystals of the V_o, to our knowledge the first two-dimensional crystals of any eukaryotic V-ATPase proton channel sector. Projection maps calculated at a resolution of ~24 Å show a ring-like structure with an asymmetric mass bound at the periphery of the ring, consistent with current structural models obtained for the holo V-ATPase from single-particle reconstructions (18, 31–33). Although the relatively small size of the crystals obtained so far has limited our ability to use cryo-electron crystallography for structural analysis, there are several features that are noteworthy at the current resolution. The diameter of the ring is, with ~8.5 nm, virtually identical to the diameter of the K subunit ring of the related sodium V-like ATPase from *E. hirae* (K_{10}, 8.3 nm (48)). This is consistent with the now established stoichiometry of 10 proteolipids for the yeast V-ATPase proteolipid ring (18), eight of which are *c* subunits (Vma3p), with each one copy of *c′* (Vma11p) and *c″* (Vma16p) (17) to give a complex of $c_8c'c''$. Another observation from the two-dimensional crystal projection is that a_{CT} appears to be organized in two domains of slightly unequal size (Fig. 3*E*, *arrowheads*). A recent cryo-EM model of another rotary motor enzyme, the dimeric F-ATPase from *Polytomella* mitochondria revealed two almost horizontal α helices as part of the F_o-*a* subunit (58). F-ATPase F_o *a* subunits are predicted to contain five transmembrane α helices, and it is possible that the larger of the two domains observed here for V_o a_{CT} in the two-dimensional crystals represents the structural and functional homologue of F_o *a*, with the smaller of the two domains representing a part of V_o *a* that is not present in F-ATPase. Almost horizontal transmembrane α helices were also observed in a recent cryo-EM reconstruction of the holo yeast V-ATPase (18), suggesting that tilted α helices in the interface between a_{CT} and the proteolipid ring are a conserved feature in all rotary motor enzymes.

Because the current two-dimensional crystals are too small to generate a three-dimensional structural model from images of a tilted specimen, we used cryo-electron microscopy of detergent-solubilized single V_o sectors to calculate a three-dimensional reconstruction of the complex using our earlier negative-stain, three-dimensional EM reconstruction of the bovine V_o (29) as a starting model. Although the resolution of the yeast V_o reconstruction presented here is limited to about 18 Å (likely because of the relatively small size of the V_o (~320 kDa), the presence of a featureless detergent belt, and the lack of overall symmetry), the EM density allows placing of the crystal structures of equivalent subunits from related bacterial enzymes, namely the *E. hirae* K_{10} ring (48) and a_{NT} and subunit *d* homologs from *M. ruber* (50) and *T. thermophilus* (51), respectively. The resulting pseudo-atomic model shows a_{NT} and subunit *d* in close proximity, suggesting that the two polypeptides bind each other in free V_o, consistent with what had already been described for the bovine complex (29, 57). However, the cryo-EM model of yeast V_o presented here provides more detail by showing the tether connecting a_{NT} and a_{CT} that was not resolved in the bovine model (29). Interestingly, a comparison of EM reconstructions of free V_o and V_o as part of holo V-ATPase (Fig. 4*D*) revealed that a_{NT} must undergo a large conformational change during regulated enzyme disassembly, from a conformation in holo V-ATPase, where the distal domain of a_{NT} binds C_{foot} and EG2 (18, 31, 44), to a conformation in free V_o, where a_{NT} binds subunit *d*. As mentioned above, we initially reasoned that the a_{NT}-*d* interaction may play a role in blocking passive proton conductance. However, as summarized in Fig. 6, removal of subunit *d* by the ionic detergent LPPG to produce $V_o\Delta d$, followed by proton conductance assays, showed no difference in the behavior of the V_o and $V_o\Delta d$ complexes. This result suggests that the interaction of *d* with a_{NT} is not (solely) responsible for blocking proton flow across free V_o, consistent with earlier experiments by Qi and Forgac (34) that showed that proteolytic removal of a_{NT} on vacuolar vesicles did not render the membrane permeable to protons. Taken together, this means that there must be other (or additional) mechanisms that prevent proton leakage through free V_o. As illustrated in Fig. 7, one possibility is that the conformational change in a_{NT} upon enzyme dissociation is transmitted to a_{CT}, thereby disrupting the path of protons along the interface between a_{CT} and the proteolipid ring. Another mechanism for blocking passive proton transport could lie within the structure of the proteolipid ring itself. V-ATPase proteolipids have four transmembrane α helices but only one essential proton carrying carboxylate (59), resulting in a larger distance between proton binding sites compared with F-ATP synthase. The large gap between proton binding sites (Fig. 7) could represent too high of a barrier to overcome without the driving force from ATP hydrolysis, resulting in kinetic inhibition of proton flow from the vacuole into the cytoplasm.

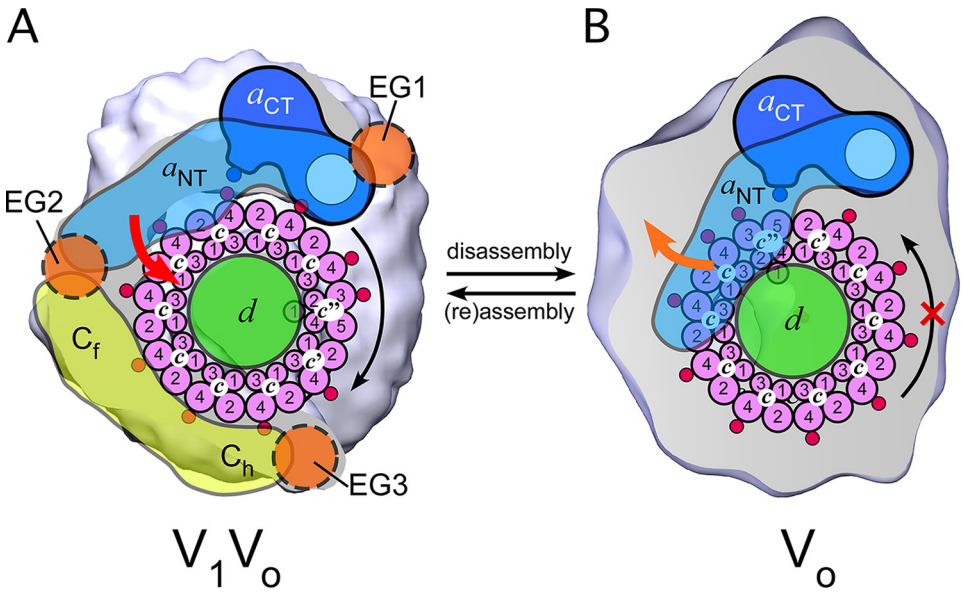

FIGURE 7. **Structural rearrangement of a_{NT} upon reversible disassembly and mechanism of activity silencing.** *A* and *B*, comparison of cross-sections of the three-dimensional EM reconstructions of (*A*) yeast V_1V_o (emd-5476) and (*B*) isolated V_o at the level of a_{NT}. In holo V_1V_o, the distal domain of a_{NT} is in contact with the foot domain of subunit C (C_f) and the N-terminal domain of peripheral stalk EG2. Release of V_1 from V_o upon enzyme disassembly results in a large movement of a_{NT} away from its peripheral position near C_f and EG2 to bind subunit *d* (*A*, *red arrow*). Upon (re)assembly, the interaction between a_{NT} and *d* is broken, and a_{NT} moves back to its peripheral position in the holo enzyme (*B*, *orange arrow*). In one model of activity silencing, the rearrangement of a_{NT} upon enzyme disassembly is transmitted to a_{CT}, thereby blocking passive proton transport by altering the proximity of critical residues in a_{CT} (such as Arg-745, *small blue sphere*) relative to the proton-carrying carboxyls in the *c* subunit ring (*small red spheres*). Another possibility is that passive proton transport is kinetically inhibited because of the larger distance between carboxyls in the V-ATPase proteolipid ring compared with F-ATPase. Note that an even larger gap between carboxyls is predicted because of the proteolipid isoform *c*″, which has the essential glutamate in transmembrane α helix 3 (Glu-108) as opposed to in helix 4 as for *c* (Glu-137) and *c*′ (Glu-145) (59, 62, 63). For details, see text.

However, if the a_{NT}-*d* interaction in free V_o is not involved in blocking passive proton translocation, what then, if any, might its physiological role be? It has been shown that removing the tether linking a_{NT} and a_{CT} prevents assembly of holo V-ATPase (resulting in free cytoplasmic V_1 and vacuolar membrane-bound V_o that lacks subunit *d*), a defect that can be partially rescued upon overexpression of subunit *d* (60). This finding suggests that the interaction of *d* with the proteolipid ring is relatively weak and that the additional interaction with a_{NT} is needed to increase avidity for *d* during V_o biogenesis and for retaining *d* upon regulated enzyme disassembly. In line with this model is the relatively weak affinity (K_d, ~5 μM) between a_{NT} and *d*, as measured by ITC using recombinant subunits because this interaction must be readily reversible for enzyme reassembly. Interestingly, recent studies have shown that the vacuole-specific phosphoinositide $PI(3,5)P_2$ plays a role in regulating V-ATPase (re)assembly and that $PI(3,5)P_2$ is able to directly bind a_{NT} (61). One possibility is that the $PI(3,5)P_2$ headgroups compete with subunit *d* for a_{NT} binding, thereby helping to change the conformation of a_{NT} from the free V_o state to a more peripheral conformation in preparation for enzyme reassembly.

Currently, there is no high-resolution structure available for an intact membrane domain of any of the rotary motor enzymes, and this lack of structural information has limited our understanding of the mechanism of ion translocation and activity silencing in case of the eukaryotic V-ATPase. The protocol described here allows isolation of highly purified and stable V_o, paving the way for obtaining a high-resolution structure of a rotary motor ATPase proton channel sector using crystallographic or single-molecule techniques. Studies toward that aim are ongoing in our laboratory.

Author Contributions—S. C. C. and S. W. designed the study and wrote the manuscript. S. C. C. performed the V_o purification and structural characterization with technical assistance from S. W. S. W. performed the ITC experiments, including recombinant protein purification. E. M. generated the subunit B deletion strain.

Acknowledgments—We thank Dr. Patricia Kane for reagents and help with yeast molecular biology and Nicholas J. Stam, Stuti Sharma, and Dr. Rebecca A. Oot for discussions. We thank Dr. Karlett Parra for the plasmid encoding yeast V-ATPase subunit d and Dr. Lee Parsons for generating the subunit d expression construct. We also thank Robert Carroll for generating the $a_{NT(1–372)}$ expression construct and Dr. Richard Gillilan for help with BioSAXS data collection. Part of this work is on the basis of research conducted at the Cornell High-Energy Synchrotron Source (CHESS), which is supported by the National Science Foundation and the NIGMS/National Institutes of Health under National Science Foundation Award DMR-1332208, using the Macromolecular Diffraction at CHESS (MacCHESS) facility, which is supported by Award GM-103485 from the NIGMS/National Institutes of Health.

References

1. Forgac, M. (2007) Vacuolar ATPases: rotary proton pumps in physiology and pathophysiology. *Nat. Rev. Mol. Cell Biol.* **8,** 917–929
2. Kane, P. M. (2007) The long physiological reach of the yeast vacuolar H^+-ATPase. *J. Bioenerg. Biomembr.* **39,** 415–421
3. Sun-Wada, G. H., Wada, Y., and Futai, M. (2004) Diverse and essential roles of mammalian vacuolar-type proton pump ATPase: toward the

physiological understanding of inside acidic compartments. *Biochim. Biophys. Acta* **1658,** 106–114
4. Blake-Palmer, K. G., and Karet, F. E. (2009) Cellular physiology of the renal H^+ATPase. *Curr. Opin. Nephrol. Hypertens.* **18,** 433–438
5. Smith, A. N., Skaug, J., Choate, K. A., Nayir, A., Bakkaloglu, A., Ozen, S., Hulton, S. A., Sanjad, S. A., Al-Sabban, E. A., Lifton, R. P., Scherer, S. W., and Karet, F. E. (2000) Mutations in ATP6N1B, encoding a new kidney vacuolar proton pump 116-kD subunit, cause recessive distal renal tubular acidosis with preserved hearing. *Nat. Genet.* **26,** 71–75
6. Karet, F. E., Finberg, K. E., Nelson, R. D., Nayir, A., Mocan, H., Sanjad, S. A., Rodriguez-Soriano, J., Santos, F., Cremers, C. W., Di Pietro, A., Hoffbrand, B. I., Winiarski, J., Bakkaloglu, A., Ozen, S., Dusunsel, R., Goodyer, P., Hulton, S. A., Wu, D. K., Skvorak, A. B., Morton, C. C., Cunningham, M. J., Jha, V., and Lifton, R. P. (1999) Mutations in the gene encoding B1 subunit of H^+-ATPase cause renal tubular acidosis with sensorineural deafness. *Nat. Genet.* **21,** 84–90
7. Thudium, C. S., Jensen, V. K., Karsdal, M. A., and Henriksen, K. (2012) Disruption of the V-ATPase functionality as a way to uncouple bone formation and resorption: a novel target for treatment of osteoporosis. *Curr. Protein Pept. Sci.* **13,** 141–151
8. Sun-Wada, G. H., Toyomura, T., Murata, Y., Yamamoto, A., Futai, M., and Wada, Y. (2006) The a3 isoform of V-ATPase regulates insulin secretion from pancreatic β-cells. *J. Cell Sci.* **119,** 4531–4540
9. Wong, D., Bach, H., Sun, J., Hmama, Z., and Av-Gay, Y. (2011) *Mycobacterium tuberculosis* protein tyrosine phosphatase (PtpA) excludes host vacuolar-H^+-ATPase to inhibit phagosome acidification. *Proc. Natl. Acad. Sci. U.S.A.* **108,** 19371–19376
10. Lu, X., Yu, H., Liu, S. H., Brodsky, F. M., and Peterlin, B. M. (1998) Interactions between HIV1 Nef and vacuolar ATPase facilitate the internalization of CD4. *Immunity* **8,** 647–656
11. Brown, D., Smith, P. J., and Breton, S. (1997) Role of V-ATPase-rich cells in acidification of the male reproductive tract. *J. Exp. Biol.* **200,** 257–262
12. Sennoune, S. R., Bakunts, K., Martínez, G. M., Chua-Tuan, J. L., Kebir, Y., Attaya, M. N., and Martínez-Zaguilán, R. (2004) Vacuolar H^+-ATPase in human breast cancer cells with distinct metastatic potential: distribution and functional activity. *Am. J. Physiol. Cell Physiol.* **286,** C1443–1452
13. Johnson, R. M., Allen, C., Melman, S. D., Waller, A., Young, S. M., Sklar, L. A., and Parra, K. J. (2010) Identification of inhibitors of vacuolar proton-translocating ATPase pumps in yeast by high-throughput screening flow cytometry. *Anal. Biochem.* **398,** 203–211
14. Kartner, N., and Manolson, M. F. (2014) Novel techniques in the development of osteoporosis drug therapy: the osteoclast ruffled-border vacuolar H^+-ATPase as an emerging target. *Expert. Opin. Drug Discov.* **9,** 505–522
15. Fais, S., De Milito, A., You, H., and Qin, W. (2007) Targeting vacuolar H^+-ATPases as a new strategy against cancer. *Cancer Res.* **67,** 10627–10630
16. Kitagawa, N., Mazon, H., Heck, A. J., and Wilkens, S. (2008) Stoichiometry of the peripheral stalk subunits E and G of yeast V1-ATPase determined by mass spectrometry. *J. Biol. Chem.* **283,** 3329–3337
17. Powell, B., Graham, L. A., and Stevens, T. H. (2000) Molecular characterization of the yeast vacuolar H^+-ATPase proton pore. *J. Biol. Chem.* **275,** 23654–23660
18. Zhao, J., Benlekbir, S., and Rubinstein, J. L. (2015) Electron cryomicroscopy observation of rotational states in a eukaryotic V-ATPase. *Nature* **521,** 241–245
19. Arai, S., Saijo, S., Suzuki, K., Mizutani, K., Kakinuma, Y., Ishizuka-Katsura, Y., Ohsawa, N., Terada, T., Shirouzu, M., Yokoyama, S., Iwata, S., Yamato, I., and Murata, T. (2013) Rotation mechanism of *Enterococcus hirae* V1-ATPase based on asymmetric crystal structures. *Nature* **493,** 703–707
20. Kawasaki-Nishi, S., Nishi, T., and Forgac, M. (2001) Arg-735 of the 100-kDa subunit a of the yeast V-ATPase is essential for proton translocation. *Proc. Natl. Acad. Sci. U.S.A.* **98,** 12397–12402
21. Muench, S. P., Trinick, J., and Harrison, M. A. (2011) Structural divergence of the rotary ATPases. *Q. Rev. Biophys.* **44,** 311–356
22. Wilkens, S. (2005) Rotary molecular motors. *Adv. Protein Chem.* **71,** 345–382
23. Stewart, A. G., Sobti, M., Harvey, R. P., and Stock, D. (2013) Rotary ATPases: models, machine elements and technical specifications. *Bioarchitecture* **3,** 2–12
24. Sumner, J. P., Dow, J. A., Earley, F. G., Klein, U., Jäger, D., and Wieczorek, H. (1995) Regulation of plasma membrane V-ATPase activity by dissociation of peripheral subunits. *J. Biol. Chem.* **270,** 5649–5653
25. Kane, P. M. (1995) Disassembly and reassembly of the yeast vacuolar H+-ATPase *in vivo*. *J. Biol. Chem.* **270,** 17025–17032
26. Parra, K. J., Keenan, K. L., and Kane, P. M. (2000) The H subunit (Vma13p) of the yeast V-ATPase inhibits the ATPase activity of cytosolic V1 complexes. *J. Biol. Chem.* **275,** 21761–21767
27. Gräf, R., Harvey, W. R., and Wieczorek, H. (1996) Purification and properties of a cytosolic V1-ATPase. *J. Biol. Chem.* **271,** 20908–20913
28. Diab, H., Ohira, M., Liu, M., Cobb, E., and Kane, P. M. (2009) Subunit interactions and requirements for inhibition of the yeast V1-ATPase. *J. Biol. Chem.* **284,** 13316–13325
29. Wilkens, S., and Forgac, M. (2001) Three-dimensional structure of the vacuolar ATPase proton channel by electron microscopy. *J. Biol. Chem.* **276,** 44064–44068
30. Wilkens, S., Inoue, T., and Forgac, M. (2004) Three-dimensional structure of the vacuolar ATPase: localization of subunit H by difference imaging and chemical cross-linking. *J. Biol. Chem.* **279,** 41942–41949
31. Zhang, Z., Zheng, Y., Mazon, H., Milgrom, E., Kitagawa, N., Kish-Trier, E., Heck, A. J., Kane, P. M., and Wilkens, S. (2008) Structure of the yeast vacuolar ATPase. *J. Biol. Chem.* **283,** 35983–35995
32. Benlekbir, S., Bueler, S. A., and Rubinstein, J. L. (2012) Structure of the vacuolar-type ATPase from *Saccharomyces cerevisiae* at 11-A resolution. *Nat. Struct. Mol. Biol.* **19,** 1356–1362
33. Rawson, S., Phillips, C., Huss, M., Tiburcy, F., Wieczorek, H., Trinick, J., Harrison, M. A., and Muench, S. P. (2015) Structure of the vacuolar H^+-ATPase rotary motor reveals new mechanistic insights. *Structure* **23,** 461–471
34. Qi, J., and Forgac, M. (2008) Function and subunit interactions of the N-terminal domain of subunit a (Vph1p) of the yeast V-ATPase. *J. Biol. Chem.* **283,** 19274–19282
35. Nielsen, S. S., Toft, K. N., Snakenborg, D., Jeppesen, M. G., Jacobsen, J. K., Vestergaard, B., Kutter, J. P., Arleth, L. (2009) BioXTAS RAW, a software program for high-throughput automated small-angle X-ray scattering data reduction and preliminary analysis. *J. Appl. Cryst.* **42,** 959–964
36. Gipson, B., Zeng, X., Zhang, Z. Y., and Stahlberg, H. (2007) 2dx: user-friendly image processing for 2D crystals. *J. Struct. Biol.* **157,** 64–72
37. van Heel, M., Harauz, G., Orlova, E. V., Schmidt, R., and Schatz, M. (1996) A new generation of the IMAGIC image processing system. *J. Struct. Biol.* **116,** 17–24
38. Lee, J. Y., Urbatsch, I. L., Senior, A. E., and Wilkens, S. (2008) Nucleotide-induced structural changes in P-glycoprotein observed by electron microscopy. *J. Biol. Chem.* **283,** 5769–5779
39. Ludtke, S. J., Baldwin, P. R., and Chiu, W. (1999) EMAN: semiautomated software for high-resolution single-particle reconstructions. *J. Struct. Biol.* **128,** 82–97
40. Dube, P., Tavares, P., Lurz, R., and van Heel, M. (1993) The portal protein of bacteriophage SPP1: a DNA pump with 13-fold symmetry. *EMBO J.* **12,** 1303–1309
41. Pettersen, E. F., Goddard, T. D., Huang, C. C., Couch, G. S., Greenblatt, D. M., Meng, E. C., and Ferrin, T. E. (2004) UCSF Chimera: a visualization system for exploratory research and analysis. *J. Comput. Chem.* **25,** 1605–1612
42. Böttcher, B., Wynne, S. A., and Crowther, R. A. (1997) Determination of the fold of the core protein of hepatitis B virus by electron cryomicroscopy. *Nature* **386,** 88–91
43. Kelley, L. A., Mezulis, S., Yates, C. M., Wass, M. N., and Sternberg, M. J. (2015) The Phyre2 web portal for protein modeling, prediction and analysis. *Nat. Protoc.* **10,** 845–858
44. Oot, R. A., and Wilkens, S. (2012) Subunit interactions at the V1-Vo interface in yeast vacuolar ATPase. *J. Biol. Chem.* **287,** 13396–13406
45. Oot, R. A., and Wilkens, S. (2010) Domain characterization and interaction of the yeast vacuolar ATPase subunit C with the peripheral stator stalk subunits E and G. *J. Biol. Chem.* **285,** 24654–24664
46. Peterson, G. L. (1977) A simplification of the protein assay method of Lowry *et al.* which is more generally applicable. *Anal. Biochem.* **83,**

346–356
47. Zhang, Z., Inoue, T., Forgac, M., and Wilkens, S. (2006) Localization of subunit C (Vma5p) in the yeast vacuolar ATPase by immuno electron microscopy. *FEBS Lett.* **580,** 2006–2010
48. Murata, T., Yamato, I., Kakinuma, Y., Leslie, A. G., and Walker, J. E. (2005) Structure of the rotor of the V-Type Na^+-ATPase from *Enterococcus hirae*. *Science* **308,** 654–659
49. Compton, M. A., Graham, L. A., and Stevens, T. H. (2006) Vma9p (subunit e) is an integral membrane V0 subunit of the yeast V-ATPase. *J. Biol. Chem.* **281,** 15312–15319
50. Srinivasan, S., Vyas, N. K., Baker, M. L., and Quiocho, F. A. (2011) Crystal structure of the cytoplasmic N-terminal domain of subunit I, a homolog of subunit a, of V-ATPase. *J. Mol. Biol.* **412,** 14–21
51. Iwata, M., Imamura, H., Stambouli, E., Ikeda, C., Tamakoshi, M., Nagata, K., Makyio, H., Hankamer, B., Barber, J., Yoshida, M., Yokoyama, K., and Iwata, S. (2004) Crystal structure of a central stalk subunit C and reversible association/dissociation of vacuole-type ATPase. *Proc. Natl. Acad. Sci. U.S.A.* **101,** 59–64
52. Drory, O., Frolow, F., and Nelson, N. (2004) Crystal structure of yeast V-ATPase subunit C reveals its stator function. *EMBO Rep.* **5,** 1148–1152
53. Schneider, E., and Altendorf, K. (1985) All three subunits are required for the reconstitution of an active proton channel (F0) of *Escherichia coli* ATP synthase (F1F0). *EMBO J.* **4,** 515–518
54. Mosher, M. E., Peters, L. K., and Fillingame, R. H. (1983) Use of λ unc transducing bacteriophages in genetic and biochemical characterization of H^+-ATPase mutants of *Escherichia coli*. *J. Bacteriol.* **156,** 1078–1092
55. Zhang, J., Myers, M., and Forgac, M. (1992) Characterization of the V0 domain of the coated vesicle H^+-ATPase. *J. Biol. Chem.* **267,** 9773–9778
56. Suzuki, T., Ueno, H., Mitome, N., Suzuki, J., and Yoshida, M. (2002) F(0) of ATP synthase is a rotary proton channel: obligatory coupling of proton translocation with rotation of c-subunit ring. *J. Biol. Chem.* **277,** 13281–13285
57. Wilkens, S., Zhang, Z., and Zheng, Y. (2005) A structural model of the vacuolar ATPase from transmission electron microscopy. *Micron* **36,** 109–126
58. Allegretti, M., Klusch, N., Mills, D. J., Vonck, J., Kühlbrandt, W., and Davies, K. M. (2015) Horizontal membrane-intrinsic α-helices in the stator a-subunit of an F-type ATP synthase. *Nature* **521,** 237–240
59. Hirata, R., Graham, L. A., Takatsuki, A., Stevens, T. H., and Anraku, Y. (1997) VMA11 and VMA16 encode second and third proteolipid subunits of the *Saccharomyces cerevisiae* vacuolar membrane H^+-ATPase. *J. Biol. Chem.* **272,** 4795–4803
60. Ediger, B., Melman, S. D., Pappas, D. L., Jr., Finch, M., Applen, J., and Parra, K. J. (2009) The tether connecting cytosolic (N terminus) and membrane (C terminus) domains of yeast V-ATPase subunit a (Vph1) is required for assembly of V0 subunit d. *J. Biol. Chem.* **284,** 19522–19532
61. Li, S. C., Diakov, T. T., Xu, T., Tarsio, M., Zhu, W., Couoh-Cardel, S., Weisman, L. S., and Kane, P. M. (2014) The signaling lipid PI(3,5)P(2) stabilizes V_1-V_o sector interactions and activates the V-ATPase. *Mol. Biol. Cell* **25,** 1251–1262
62. Wang, Y., Cipriano, D. J., and Forgac, M. (2007) Arrangement of subunits in the proteolipid ring of the V-ATPase. *J. Biol. Chem.* **282,** 34058–34065
63. Wang, Y., Inoue, T., and Forgac, M. (2004) TM2 but not TM4 of subunit c″ interacts with TM7 of subunit a of the yeast V-ATPase as defined by disulfide-mediated cross-linking. *J. Biol. Chem.* **279,** 44628–44638